Autonomous Navigation and Attitude Determination System Design for Micro-Nano Satellites with Limited Sensors

Chaoyu Du[1], Tao Meng[2,3(✉)], Jun Wang[4], and Zhonghe Jin[2,3]

[1] School of Information Science and Electrical Engineering, Zhejiang University, Hangzhou 310027, China

[2] School of Aeronautics and Astronautics, Zhejiang University, Hangzhou 310027, China
mengtao@zju.edu.cn

[3] China Micro-Nano Satellite Research Laboratory of Zhejiang Province, Hangzhou 310027, China

[4] Operations Center, China Satellite Communications, Beijing 100190, China

Abstract. Autonomous system design has received extensive attention for orbit and attitude determination, since the traditional ground station-based orbit determination is difficult to meet the multi-satellite needs. With a combination of limited sensors, this article presents an autonomous navigation-attitude determination system for low-earth-orbit micro-nano satellites. By adding the area-to-mass ratio to state vector, the atmospheric resistance is effectively considered. By introducing an infrared earth sensor, the limitations of the orbit type and eclipse period are compensated, with the consideration of computational burden. Simulation based on ZDPS-2 satellites show the estimation accuracy of this paper is improved by 23% compared with the magnetometer/sun sensor combination, reaching 1.08 km, 1.16 m/s (RMS); whereas for an equatorial orbit, estimation accuracy remains 1.11 km (RMS). While completing navigation estimation, the system attitude pointing accuracy reaches 0.347° (RMS), which meets the basic mission requirements of micro-nano satellites.

Keywords: Navigation · Magnetometer · Earth sensor · Micro-nano satellite

1 Introduction

A growing interest has been expressed in micro-nano satellites which offer advantages such as low cost, short development period and standard with large quantities. For the attitude control system, orbital parameters are an indispensable input for any attitude determination algorithm. The traditional ground station-based orbit determination is difficult to meet the multi demands as formation flying plays a more important role in space missions. Therefore, autonomous operating system design has received extensive attention for orbit and attitude determination.

H. Ding (ed.), *Aerospace Mechatronics and Control Technology*, Springer Aerospace Technology,
https://doi.org/10.1007/978-981-16-6640-7_14

Navigation based on GPS/GNSS or star sensor, has been popular among recent research [1–3]. Whereas for micro-nano satellites which are equipped with limited sensors, it can be useful explorations on autonomous determination, if no additional sensitive components are added.

Since the magnetometer-based satellite navigation was first proposed by research team at Cornell, studies have been carried out focusing on geomagnetic navigation. The scalar magnitude of the magnetic field was introduced as measurement vector to establish the orbit determination [4]. A state estimator for a low-earth near-polar orbit reached a position accuracy of 2.5–3 km [5]. Further discussions were made by analyzing the basis of the accuracy effects, such as dynamic model, orbit types, measurement calibration, and linearization of measurement model [6].

In order to further improve system accuracy, Psiaki was among the pioneers who added sun sensor data to the geomagnetic navigation system [7], and with the measured magnetic field data of DE-2, MAGSAT, and LACE satellites [8], a batch filter and EKF algorithm reached an position error of 2.19 km, but the integrated system showed low accuracy in eclipse. Compared with EKF, a particle filter was verified and showed similar position accuracy, but better convergence rate [9]. Simplifications were introduced and testified on Jacobian calculations and polynomial model for fast magnetic field calculation [10]. Calibrations on bias and scale factors of the magnetometer were discussed [11]. By introducing a horizon sensor with UKF, a less than 500 m accuracy of position and less than 1 m/s accuracy in velocity are found with 0.1 nT magnetometer and 0.05° horizon/earth sensor [12].

The second approach for magnetometer measurements in dual estimation, on the other hand, choose the three-axis magnetic vector measurements instead of the scalar magnitude to perform the coupled navigation and attitude determination [13–16]. While the current attitude is needed when measurements are within the coordinate body system, a series–parallel hybrid determination strategy based on both magnitude and vector was proposed, in which the error covariance matrix was utilized as the switch [15].

However, there is lack of consideration fully focused on low-earth-orbit micro-nano satellites, as well as computational burden, to get fully use of the limited equipped sensors while meeting a proper system accuracy.

In this paper, based on the commonly equiped attitude devices: magnetometer, sun sensor and infrared earth sensor, an autonomous navigation-attitude determination system (low power consumption, full orbit, full time) is proposed. The solution excludes the considerations of low-earth perturbation, influence of orbit inclination, sub-system independence, as well as sensor redundancy. Finally, through simulation based on ZDPS-2 satellites, the proposed algorithm and system design is verified.

2 Design Guidelines

In this section, analyses on orbital perturbation, orbital inclination, measurement form of the magnetic field are given for low-earth-orbit satellites, which provides a design guideline for the navigation estimator and the combined determination system.

(1) **Atmospheric perturbation** cannot be ignored.
The orbital acceleration due to perturbation such as geopotential and atmospheric drag, the solar radiation pressure, and the sun and moon's gravity are calculated. The following table shows a calculation based on a 25 kg satellite with a 0.4 m^2 windward area.

As shown in Table 1, the non-spherical perturbation of the Earth has the greatest impact. For low-earth orbit satellites (400–600 km), the impact of atmospheric drag perturbation cannot be ignored. Therefore, the ballistic coefficient of the satellite is required to be estimated [6], which equals to the product of the drag coefficient and the area-to-mass ratio.

Table 1. Orbital perturbation

Perturbation	Orbit (400 km)	Orbit (1000 km)
J2	10^{-3}	10^{-3}
Other non-spherical	10^{-6}	10^{-6}
Atmospheric drag	2×10^{-6}	10^{-9}
Solar radiation pressure	10^{-9}	10^{-9}
Solar gravitational attractions	3×10^{-8}	5×10^{-8}

(2) **Orbital description** method.
The estimated state of the autonomous navigation filter can be the satellite Cartesian coordinate position, velocity vector [4, 6], the six Keplerian orbital elements [12], and other parameters forms. In contrast, the Keplerian form is easier for orbit description, and more suitable for calculation of the earth's magnetic field, but it requires a large amount of computing resources. On the other hand, the Cartesian form is more convenient for numerical integration.

(3) **Different orbital inclinations** need to be considered.
A magnetometer-based orbit determination is based on the principle that the distribution of the geomagnetic field along the orbit has adequate resolution to identify the specific orbit. Therefore, the data range of the geomagnetic field along the orbit should be large enough to allow a precise orbit reconstruction [6]. The range of the measured data is highly dependent on the type of orbit.

A verification simulation is set on a 500 km orbit (eccentricity = 0), with a 10 nT magnetometer. The filtering estimation result is shown in Fig. 1. When the orbital inclination is 90°, the position estimation accuracy is better than 5 km; while the error increases as the orbital inclination becomes closer to zero, due to

the low variation of the equatorial geomagnetic field. As a result, the evaluation of a magnetometer-based navigation system, should be verified at different orbit inclinations.

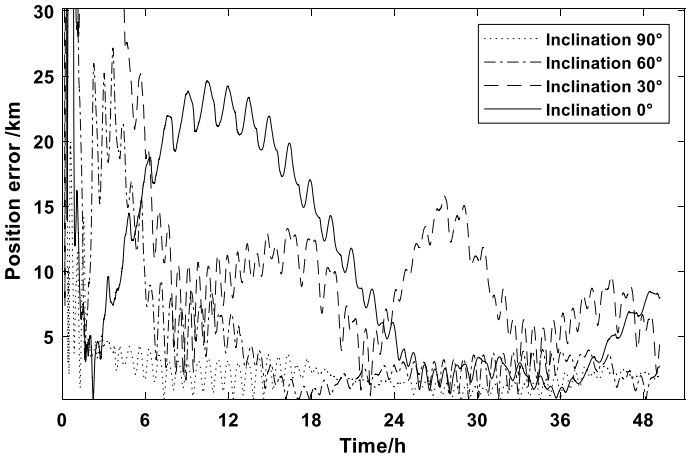

Fig. 1. Evolution of the position errors for different orbital inclinations

(4) **Convergence** of the coupled determination system.
When the three-axis magnetic vector measurements (excludes the knowledge of the attitude in the orbit determination) take place of the scalar magnitude, the coupled navigation-attitude system faces higher convergence rates. The larger estimation error of either sub system becomes, the longer it will take to be convergent. Results might be divergence as well [15].

3 System-Level Design

Based on the discussed design guidelines:

(1) In this paper, only the scalar magnitude of the geomagnetic is selected, to asure an attitude-independent orbit determination. System convergence, especially attitude determination, plays a very important role at early stage of the mission.
(2) An infrared earth imaging sensor was introduced as measurement to further enhance the observability of the commonly used magnetic/sun sensor combination; when the sun sensor becomes unavailable in eclipse, there are still continuous observations for information fusion.

The infrared earth sensor introduced in this article is shown in Fig. 2. The earth is projected onto the image plane and through image processing, the roll and pitch angle can be calculated by the following formula, with which the three-dimensional earth vector is obtained.

$$\alpha = \begin{cases} \arctan\left(\frac{Y_1 - Y_0}{X_1 - X_0}\right) & (Y_1 - Y_0) \le 0 \\ 360 - \arctan\left(\frac{Y_1 - Y_0}{X_1 - X_0}\right) & (Y_1 - Y_0) > 0 \end{cases} \tag{1}$$

$$\beta = \arctan\left(\frac{\sqrt{(X_1 - X_0)^2 + (Y_1 - Y_0)^2}}{f}\right)$$

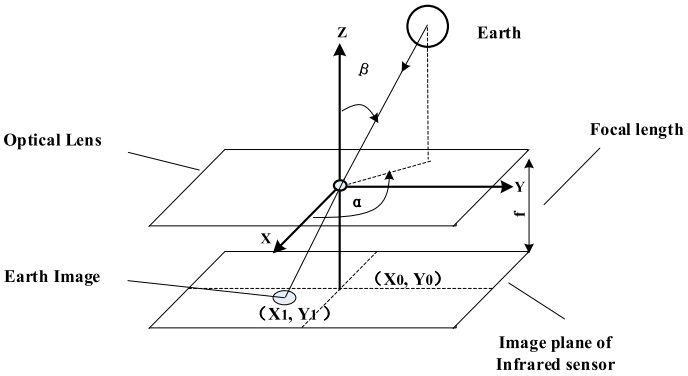

Fig. 2. Schematic principle of the static infrared earth sensor

(3) System design is shown in Fig. 3, where the fusion selector is to verify working status of the equipped sensors, they either face unavailable environment such as eclipse to sun sensor, or disabled due to self failure or under ground instructions. The status help select the latter fusion combination and algorithm.

In addition, processing of the magnetometer measurement is shown in Fig. 4, where the magnitude, and sun/earth vector angle are inputs of the navigation filter; the three-dimensional vectors are for the attitude estimator.

4 Navigation Estimator Design

The Cartesian form of coordinates is chosen for its conveniency for numerical integration. The navigation state vector is defined as follows

$$\boldsymbol{x} = \left[\boldsymbol{r}^{\mathrm{T}}\ \boldsymbol{v}^{\mathrm{T}}\ B^*\right] \tag{2}$$

where $\boldsymbol{r}$ and $\boldsymbol{v}$ are the position and velocity vectors in inertial frame, and B* is the inverse value of satellite's ballistic coefficient, which is the multiplication of the drag coefficient and the area-to-mass ratio.

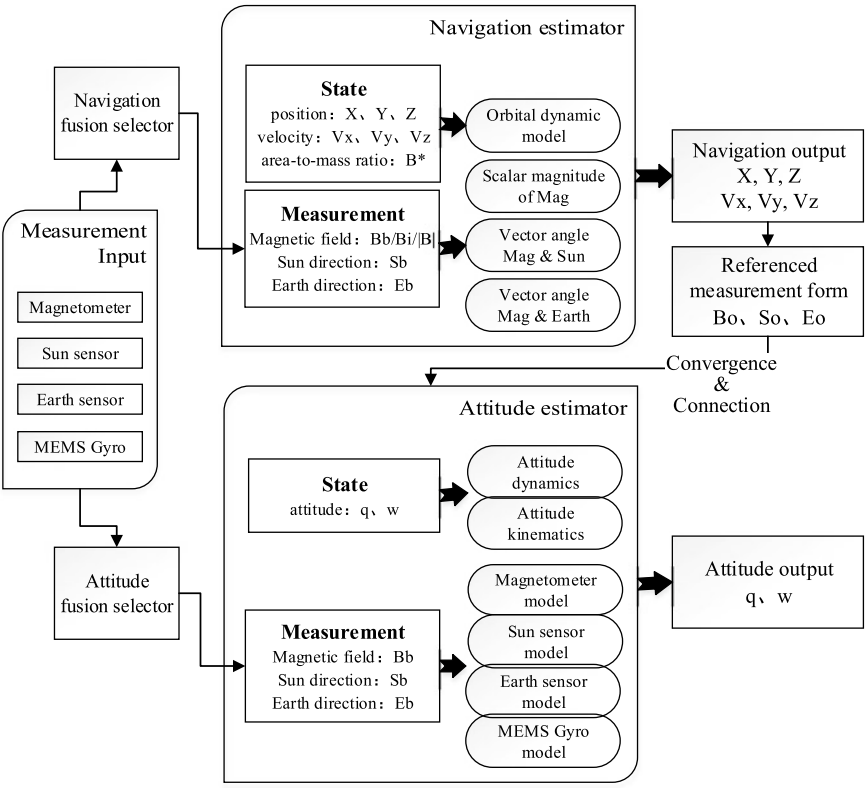

Fig. 3. System design of the autonomous navigation and attitude system

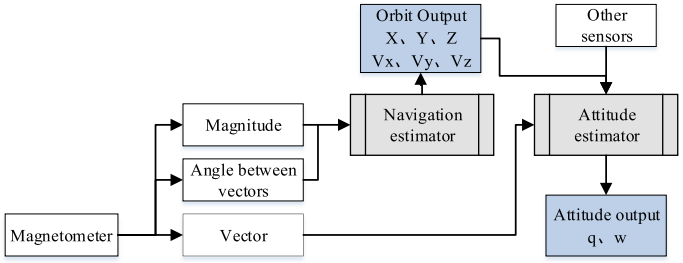

Fig. 4. Magnetometer measurement processing

4.1 Orbital Dynamic Model

The satellite, defined by multiplication of the drag coefficient and the area-to-mass ratio, and is modeled as a random walk, in which the state vector can be expressed as

$$\begin{aligned} \dot{\boldsymbol{r}} &= \boldsymbol{v} \\ \dot{\boldsymbol{v}} &= \boldsymbol{a}_{\mathrm{g}} + \boldsymbol{a}_{\mathrm{d}} + \boldsymbol{w}_1 \\ \dot{B}^{*} &= w_2 \end{aligned} \tag{3}$$

where $\boldsymbol{a}_{\mathrm{g}}$ denotes the geopotential acceleration, $\boldsymbol{a}_{\mathrm{d}}$ denotes the acceleration due to atmospheric drag. $\boldsymbol{w}_1$ an $\boldsymbol{w}_2$ are system process errors, which can be approximated as zero-mean Gaussian noise. For state propagation, can also be written as:

$$\dot{\boldsymbol{x}} = f(\boldsymbol{x}) + \boldsymbol{w} \tag{4}$$

where $\boldsymbol{w}$ denotes a combination of $\boldsymbol{w}_1$ and $\boldsymbol{w}_2$. Q is the system noise covariance matrix.

$$E\left(\boldsymbol{w}\boldsymbol{w}^{T}\right) = \boldsymbol{Q} \tag{5}$$

The Jacobian calculation of Eq. (5) can be written as

$$F(\boldsymbol{x}) = \frac{\partial f(\boldsymbol{x})}{\partial \boldsymbol{x}} = \begin{bmatrix} \boldsymbol{0}_{3\times 3} & \boldsymbol{I}_{3\times 3} & \boldsymbol{0}_{3\times 1} \\ \boldsymbol{G}_{\mathrm{r}} + \boldsymbol{D}_{\mathrm{r}} & \boldsymbol{D}_{\mathrm{v}} & \boldsymbol{D}_{\mathrm{B}} \\ \boldsymbol{0}_{1\times 3} & \boldsymbol{0}_{1\times 3} & \boldsymbol{0}_{1\times 1} \end{bmatrix} \tag{6}$$

where G_r denotes the derivative of $\boldsymbol{a}_{\mathrm{g}}$, D_r, D_v, D_B denote derivatives of $\boldsymbol{a}_{\mathrm{d}}$. Drags and J4 perturbations have been included for the orbital simulation, as well as the J2 perturbation, to obtain higher estimation accuracy with limited computational burden.

4.2 Measurement Function

Measurement model of the scalar magnitude of the geomagnetic can be written as

$$y_1 = \sqrt{\boldsymbol{B}_{\mathrm{mes}}^{\mathrm{T}}\boldsymbol{B}_{\mathrm{mes}}} \approx \sqrt{\boldsymbol{B}_{\mathrm{act}}^{\mathrm{T}}\boldsymbol{B}_{\mathrm{act}}} + n_{\mathrm{y1}} \tag{7}$$

the statistics of n_{y1} are as follows:

$$E\left(n_{\mathrm{y1}}\right) = 0, E\left(n_{\mathrm{y1}}n_{\mathrm{y1}}^{\mathrm{T}}\right) = \sigma_{\mathrm{m}}^{2} \tag{8}$$

the measured dot product of the magnetic field vector and the sun direction vector y_2, and with earth direction vector y_3, can be shown as

$$\begin{aligned} y_2 &= \boldsymbol{B}_{\text{mes}}^{\text{T}} \boldsymbol{S}_{\text{mes}} \approx \boldsymbol{B}_{\text{act}}^{\text{T}} \boldsymbol{S}_{\text{act}} + n_{\text{y2}} \\ y_3 &= \boldsymbol{B}_{\text{mes}}^{\text{T}} \boldsymbol{E}_{\text{mes}} \approx \boldsymbol{B}_{\text{act}}^{\text{T}} \boldsymbol{E}_{\text{act}} + n_{\text{y3}} \end{aligned} \tag{9}$$

the statistics of n_{y2} and n_{y2} are as follows:

$$\begin{aligned} &E\left(n_{\text{y2}}\right) = E\left(n_{\text{y3}}\right) = 0, \\ &E\left(n_{\text{y2}} n_{\text{y2}}^{\text{T}}\right) = \sigma_{\text{B}}^2 + \boldsymbol{B}_{\text{mes}}^{\text{T}} \left(\boldsymbol{I} - \boldsymbol{S}_{\text{mes}} \boldsymbol{S}_{\text{mes}}^{\text{T}}\right) \boldsymbol{B}_{\text{mes}} \sigma_{\text{S}}^2 \\ &E\left(n_{\text{y3}} n_{\text{y3}}^{\text{T}}\right) = \sigma_{\text{B}}^2 + \boldsymbol{B}_{\text{mes}}^{\text{T}} \left(\boldsymbol{I} - \boldsymbol{E}_{\text{mes}} \boldsymbol{E}_{\text{mes}}^{\text{T}}\right) \boldsymbol{E}_{\text{mes}} \sigma_{\text{E}}^2 \end{aligned} \tag{10}$$

The measurement function combined can be written as

$$\begin{aligned} \boldsymbol{y} &= h(\boldsymbol{x}) + \boldsymbol{n}_{\text{y}} \\ E\left(\boldsymbol{n}_{\text{y}} \boldsymbol{n}_{\text{y}}^{\text{T}}\right) &= \boldsymbol{R} \end{aligned} \tag{11}$$

where $\boldsymbol{n}_{\text{y}}$ is a combination of n_{y1}, n_{y2} and n_{y3}. R is the measurement error covariance matrix. The Jacobian calculation of Eq. (11) can be written as

$$H(\boldsymbol{x}) = \frac{\partial h(\boldsymbol{x})}{\partial \boldsymbol{x}} = \begin{bmatrix} \frac{\partial y_1}{\partial \boldsymbol{B}_{\text{act}}} \frac{\partial \boldsymbol{B}_{\text{act}}}{\partial \boldsymbol{r}_{\text{e}}} \frac{\partial \boldsymbol{r}_{\text{e}}}{\partial \boldsymbol{r}} & \boldsymbol{0}_{1\times 4} \\ \left(\frac{\partial \boldsymbol{B}_{\text{act}}}{\partial \boldsymbol{r}_{\text{e}}} \frac{\partial \boldsymbol{r}_{\text{e}}}{\partial \boldsymbol{r}} \boldsymbol{S}_{\text{act}}\right)^{\text{T}} & \boldsymbol{0}_{1\times 4} \\ \left(\frac{\partial \boldsymbol{B}_{\text{act}}}{\partial \boldsymbol{r}_{\text{e}}} \frac{\partial \boldsymbol{r}_{\text{e}}}{\partial \boldsymbol{r}} \boldsymbol{E}_{\text{act}}\right)^{\text{T}} & \boldsymbol{0}_{1\times 4} \end{bmatrix}_{3\times 7} \tag{12}$$

where $\boldsymbol{r}_{\text{e}}$ is the position vector in geocentric coordinates.

4.3 EKF Procedure

The dynamics of orbit can be represented as follows

$$\begin{aligned} \Delta \dot{\boldsymbol{x}}(t) &= \boldsymbol{F}(t) \Delta \boldsymbol{x}(t) + \boldsymbol{G}(t) \boldsymbol{W} \\ \Delta \boldsymbol{y}(t) &= \boldsymbol{H}(t) \Delta \boldsymbol{x}(t) + \boldsymbol{V} \end{aligned} \tag{13}$$

(1) Equation of the extrapolation value can be shown as

$$\begin{aligned} \Delta \hat{\boldsymbol{x}}_{k+1|k} &= \boldsymbol{\Phi}_k \Delta \hat{\boldsymbol{x}}_{k|k} \\ \boldsymbol{\Phi}_k &= \mathbf{I}_{9\times 9} + \boldsymbol{F}(t) T \end{aligned} \tag{14}$$

where the state transition matrix $\boldsymbol{F}$ propagates the state vector in each time step T. $\boldsymbol{H}$ is known as the observation matrix, and $\boldsymbol{G}$ maps the process noise into the state vector. $\boldsymbol{x}_k$ and $\boldsymbol{x}_{k\text{-}1}$ denote the current and previous state vectors.

(2) The covariance matrix of the extrapolation error is formulated as

$$\boldsymbol{P}_{k+1|k} = \boldsymbol{\Phi}_k \boldsymbol{P}_{k|k} \boldsymbol{\Phi}_k^{\mathrm{T}} + \boldsymbol{G}_k \boldsymbol{Q}_k \boldsymbol{G}_k^{\mathrm{T}} \tag{15}$$

where $\boldsymbol{Q}_k = \begin{bmatrix} \sigma_{\mathrm{r}}^2 \mathbf{I}_{3\times3} & \mathbf{0}_{3\times3} & \mathbf{0}_{3\times1} \\ \mathbf{0}_{3\times3} & \sigma_{\mathrm{v}}^2 \mathbf{I}_{3\times3} & \mathbf{0}_{3\times1} \\ \mathbf{0} & \mathbf{0} & \sigma_{\mathrm{B}*}^2 \mathbf{I}_{1\times1} \end{bmatrix}_{7\times7}$ is the covariance matrix of system noise $\boldsymbol{W}$.

(3) Filter-gain of EKF can be shown as

$$\boldsymbol{K}_{k+1} = \boldsymbol{P}_{k+1|k} \boldsymbol{H}_{k+1}^T \left(\boldsymbol{H}_{k+1} \boldsymbol{P}_{k+1|k} \boldsymbol{H}_{k+1}^T + \boldsymbol{R}_{k+1} \right)^{-1} \tag{16}$$

where $\boldsymbol{R}_{k+1} = \begin{bmatrix} \sigma_b^2 \mathbf{I}_{3\times3} & \mathbf{0}_{3\times3} \\ \mathbf{0}_{3\times3} & \sigma_{\mathrm{s}}^2 \mathbf{I}_{3\times3} \end{bmatrix}_{6\times6}$ is the covariance matrix of measurement noise $\boldsymbol{V}$, which has diagonal elements built of the variances of magnetometer and earth sensor measurement noises σ_b, σ_s

$$\Delta \hat{\boldsymbol{x}}_{k+1|k+1} = \boldsymbol{\Phi}_k \Delta \hat{\boldsymbol{x}}_k + \boldsymbol{K}_{k+1} [\Delta \boldsymbol{y}_{k+1} - \boldsymbol{H}_{k+1} \boldsymbol{\Phi}_k \Delta \hat{\boldsymbol{x}}_{k|k}] \tag{17}$$

$$\boldsymbol{P}_{k+1|k+1} = (\mathbf{I} - \boldsymbol{K}_{k+1} \boldsymbol{H}_{k+1}) \boldsymbol{P}_{k+1|k} \tag{18}$$

With the update of the estimation and the covariance matrix of the filtering error shown in (17) and (18), the equations given above represent the Extended Kalman Filter (EKF), which fulfils the recursive estimation.

5 Simulation

Performance of the algorithm and system design was verified based on the ZDPS-2 satellites, which were launched in September 2015. Simulations are based on the equipped and limited ADCS sensors, shown in Table 2.

Table 2. ZDPS-2 ADCS sensors

Sensor	Parameter	Value	Unit
Magnetometer	Accuracy	50	nT
Sun sensor	Accuracy	0.5	deg
Earth sensor	Range	Hemispheric	
	Accuracy	0.1	deg

The following combination types, listed in Table 3, are the simulations to be taken into consideration.

Table 3. Combination and navigation-attitude mode

	Sensor	Combination	Characteristic
1	Mag only	Minimum filter	Low accuracy, with limitations
2	Mag/Sun	ZDPS-2 in orbit	Back to scenario 1 during eclipse
3	Mag/Sun/Earth	Full-sensive	The proposed system design

5.1 Navigation Simulation

Based on the original orbit of ZDPS-2 satellites, the navigation accuracy of each sensitive combination is analyzed and compared. The orbit altitude is 524 km (with eccentricity of 0.00125), and the inclination is 97.389°. As shown in Figs. 5, 6, 7 and Table 4, when the satellite area-to-mass ratio is integrated as B* and brought into the filter state equation, the estimation accuracy is improved by 12.6%, thus the perturbation caused by atmospheric drag is effectively considered for the low-orbit satellite. The full-sensitive combination (mag/sun/earth) proposed in this paper has improved estimation accuracy by 23.0% compared with the mag/sun combination, reaching 1.08 km, 1.16 m/s (RMS); due to the addition of new independent measurement, the improved observability shortens the filter convergence rate from 3.1 h to 1.4 h. Compared to the mag/earth combination, the full-sensitive combination has limited accuracy improvement, but has stronger fault tolerance and anti-interference ability.

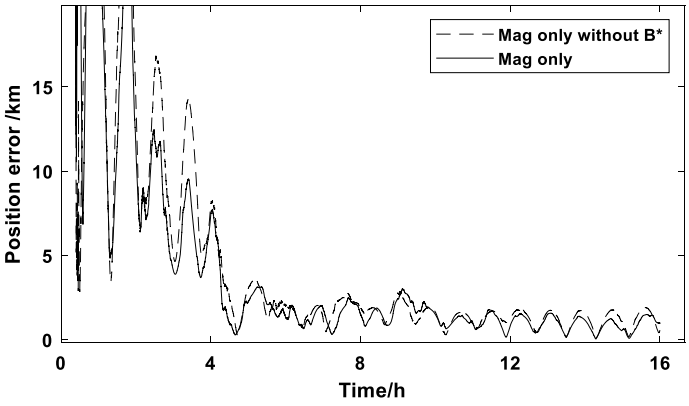

Fig. 5. Comparison with state vector B* at 97° inclination

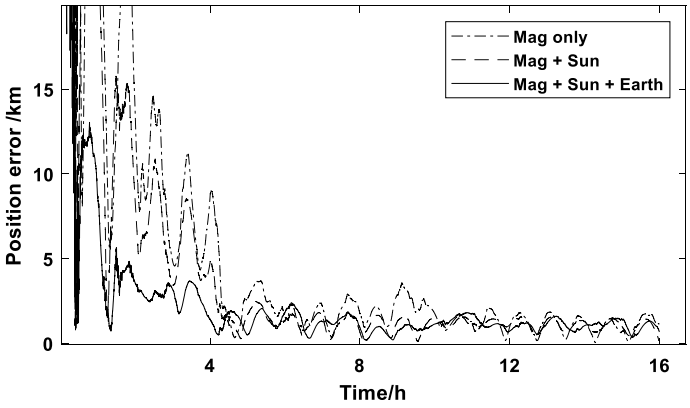

Fig. 6. Position estimation accuracy at 97° inclination

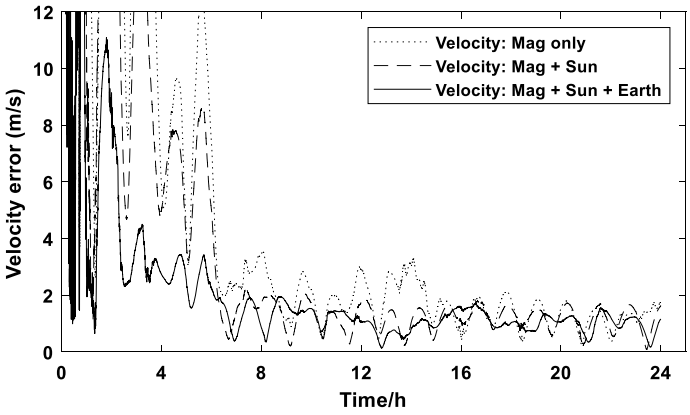

Fig. 7. Velocity estimation accuracy at 97° inclination

Table 4. Position and Velocity estimation accuracy of the navigation system

No.	Sensor	Position estimation accuracy			Velocity estimation accuracy	
		RMS/km	Max/km	Convergence (5 km)	RMS (m/s)	Max (m/s)
1	Mag (without B*)	1.637	4.378	4.2 h	1.801	3.621
2	Mag	1.454	4.161	4.2 h	1.648	3.555
3	Mag + Sun	1.328	2.868	3.1 h	1.289	2.197
4	Mag + Earth	1.105	2.376	1.5 h	1.194	2.043
5	Mag + Sun + Earth	1.078	2.319	1.4 h	1.158	1.960

The comparison simulation group carried out at the orbital inclination of 0°, as shown in Fig. 8 and Table 5. The position accuracy of the mag/sun combination becomes 10.45 km (RMS), due to the 1/3 eclipse period; however the fully-sensitive combination proposed in this paper remains 1.11 km (RMS).

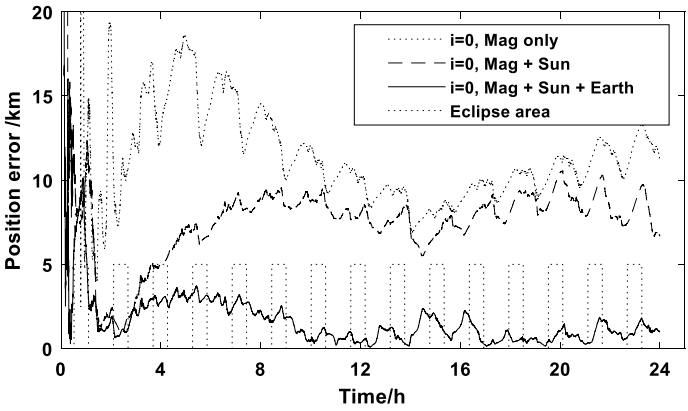

Fig. 8. Position estimation accuracy at 0° inclination

Table 5. Navigation accuracy at 0° orbit inclination

Sensor	Navigation accuracy (Position error)	
	RMS/km	Max/km
Mag	10.447	16.166
Mag + Sun	8.238	10.572
Mag + Sun + Earth	1.105	2.553

5.2 System Simulation

After the convergence of the navigation sub-system, the full-sensitive attitude filter are calculated with the prior information of the orbit estimation. System estimation error are summarized in Fig. 9 and Table 6. The accuracy of the attitude determination is improved within the full orbit range to 0.347° (RMS). The results show that the navigation and attitude determination system proposed in this paper are full orbit autonomous, with the navigation accuracy of 1.08 km and 1.16 m/s, while the three-axis pointing accuracy meets the basic mission requirements of micro-nano satellites.

6 Conclusion

A full-sensive autonomous navigation and attitude determination system is proposed. With the low-earth-orbit navigation considerations, and without the ground staion support or any other high-precision sensitive components added, the proposed algorithm and

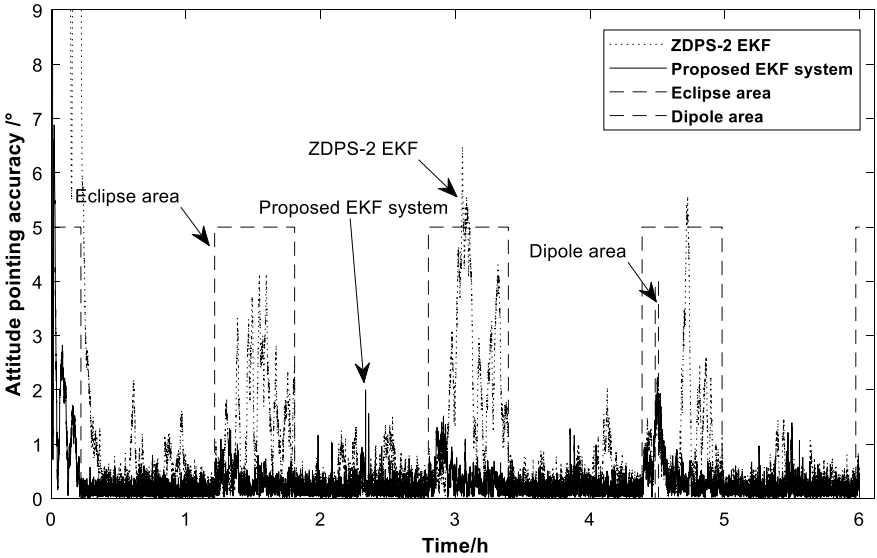

Fig. 9. Autonomous system attitude pointing accuracy

Table 6. Summary of improved filter estimation accuracy for the combined navigation and attitude system

No.	Sensor	Navigation accuracy/km (RMS)		Attitude accuracy/°(RMS)		
		RMS/km	Max/km	Sun	Eclipse	Dipole
1	Mag	1.454	4.161	2.8243		
2	Mag + Sun	1.328	2.868	1.633	/	1.633
3	Mag + Earth	1.105	2.376	0.553		/
4	Full-sensive	1.078	2.319	0.347		

system meets the basic platform requirements, and can be a useful exploration for the integration, improvement and practical design of the Micro-nano satellites navigation attitude system.

Acknowledgements. This work was supported by Primary Research and Development Plan of Zhejiang Province, key technologies of Nano remote sensing satellites, 209C05004; Zhejiang Provincial Key Laboratory of Micro-nano Satellite.

References

1. Groves PD (2015) Principles of GNSS, inertial, and multisensor integrated navigation systems. IEEE Aerosp Electron Syst Mag 30(02):26–27
2. Ning X, Wang L, Bai X, Fang J (2013) Autonomous satellite navigation using starlight refraction angle measurements. Adv Space Res 51(09):1761–1772
3. Zhang Y, Fang JC (2003) Study of the satellite autonomous celestial navigation based on the unscented kalman filter. J Astronaut 24(06):646–650
4. Psiaki ML, Huang L, Fox SM (1993) Ground tests of magnetometer-based autonomous navigation (MAGNAV) for low-earth-orbiting spacecraft. J Guid Control Dyn 16(01):206–214
5. Kim Y, Vukovich G (2014) Satellite orbit and attitude estimation using three-axis magnetometer. Int J Space Sci Eng 2(03):276–304
6. Roh KM, Park SY, Choi KH (2007) Orbit determination using the geomagnetic field measurement via the unscented Kalman filter. J Spacecr Rocket 44(01):246–253
7. Psiaki ML (1999) Autonomous low-earth-orbit determination from magnetometer and sun sensor data. J Guid Control Dyn 22(02):296–304
8. Jung H, Psiaki ML (2002) Tests of magnetometer/sun-sensor orbit determination using flight data. J Guid Control Dyn 25(03):582–590
9. Xie X, Zhang R, Zhang J (2009) Satellite autonomous orbit determination based on magnetometers and sun sensors. J Astronaut 30(03):919–923
10. Ke H, Hao W, Binjie T, Zhonghe J (2011) Pico-satellite autonomous navigation with magnetometer and sun sensor data. Chin J Aeronaut 24(01):46–54
11. Juang JC, Tsai YF, Tsai CT (2012) Design and verification of a magnetometer-based orbit determination and sensor calibration algorithm. Aerosp Sci Technol 21(01):47–54
12. Farahanifar M, Assadian N (2015) Integrated magnetometer–horizon sensor low-earth orbit determination using UKF. Acta Astronaut 106:13–23
13. Abdelrahman M, Park SY (2011) Simultaneous spacecraft attitude and orbit estimation using magnetic field vector measurements. Aerosp Sci Technol 15(08):653–669
14. Peng W, Yingchun Z (2014) J Chinese Inertial Technol 22(06):741–747
15. Xing Y, Zhang S, Cao X (2009) Determination of integrated orbit and attitude of satellite based on geomagnetic field measurements. J Harbin Inst Technol 41(07):11–15
16. Zhang T, Zheng J, Gao D (2017) A method of autonomous navigation using the magnetometer and star sensor. J Astronaut 38(02):152–158